Dynamics of feedback controlled photorefractive beam coupling

E. V. Podivilov and B. I. Sturman*
Institute of Automation and Electrometry of the Russian Academy of Science, Koptyug Avenue 1, 630090 Novosibirsk, Russia

S. G. Odoulov,† S. Pavlyuk, and K. V. Shcherbin
Institute of Physics, National Academy of Science, 252650 Kiev, Ukraine

V. Ya. Gayvoronsky,‡ K. H. Ringhofer,§ and V. P. Kamenov
Department of Physics, University of Osnabrück, D-49069 Osnabrück, Germany
(Received 12 September 2000; published 12 April 2001)

We investigate theoretically and experimentally the operation of a nonlinear system, feedback controlled photorefractive beam coupling. It is shown that the feedback equations used earlier ($\pm\pi/2$ phase shift between the diffracted and transmitted beam components) are satisfactory only during a relatively short initial stage of development. We have generalized these equations by taking into account the inertia inherent in any real feedback loop. The inertial feedback equations ensure the permanent operation of the nonlinear system and lead to a variety of periodic and quasiperiodic regimes. We investigate the distinctive features of these regimes and transitions between them for moderately thick crystals. Good qualitative agreement between theory and experimental data is obtained for $LiNbO_3$ crystals.

DOI: 10.1103/PhysRevA.63.053805 PACS number(s): 42.65.Hw, 42.65.Sf

I. INTRODUCTION

Several new exciting research areas, such as spatial solitons [1], pattern formation [2], subharmonic generation [3], feedback controlled beam coupling, arose in the field of photorefractive nonlinear phenomena during the recent years. The last of these topics stands separately in this list in the sense that it has, to our best knowledge, no direct analogs among the known nonlinear wave phenomena. This is greatly due to the distinctive feature of the photorefractive nonlinearity, namely, its relatively big inertia that allows us to send a controlling electronic signal from output to input without any big delay.

The history of the studies of the feedback controlled wave coupling is rather short. Initially, in the beginning of the nineties it was found empirically [4–6] that a certain electronic feedback loop between the output and input signal beams, governing the input phase φ_s, see Fig. 1, produces remarkable changes in the dynamics of two-wave (2W) coupling and in the diffractive properties of the recorded spatial refractive index grating. In particular, the grating could persist almost diffractive or transparent, whereas mechanical instabilities, inherent in many photorefractive experiments, could be strongly suppressed. The interpretation of the experimental results was initially based on the assumption of a uniform spatial grating whose amplitude is constant across the crystal and whose fringes are not bent. Unfortunately, this simplifying assumption is not compatible with the basic relations of photorefractive beam coupling.

A general formulation of the feedback problem, including the equations governing beam coupling, boundary conditions, and arbitrary distortions of the grating fringes, has been achieved in 1997 [7]. It has established the basis for the subsequent development. Despite of their apparent simplicity, the formulated equations occurred to be rather resistant against the application of analytical tools and methods of qualitative analysis. This is caused, in turn, by the peculiarity of the situation in question, where the temporal development of a strongly nonlinear distributed system is governed by strongly nonlinear feedback conditions coupling the opposite faces of the crystal.

The progress made after formulation of the nonlinear problem was based greatly on numerical simulations [7]. It was shown that, in accordance with experiment, the feedback

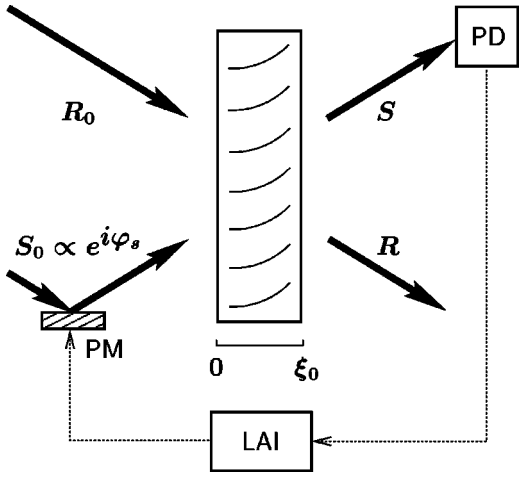

FIG. 1. Scheme of an experiment on feedback controlled photorefractive two-beam coupling: PD is a photodiode, LAI denotes a lock-in amplifier and integrator, PM is a piezomounted mirror adjusting the input phase φ_s.

*Email address: sturman@iae.nsk.su
†Email address: odoulov@iop.kiev.ua
‡Permanent address: Institute of Physics, National Academy of Sciences, 252650 Kiev, Ukraine.
§Email address: ringhofe@uos.de

 ©2001 The American Physical Society

leads the system to a state with $\eta=1$ or 0 (η is the diffraction efficiency of the grating) where the feedback signal turns to zero. In other words, the formulated mathematical problem remains correct only within a restricted time interval. Further evolution of the system cannot be investigated within the formulated feedback conditions that will be referred to as the ideal feedback conditions.

An important study relevant to the subject has recently been presented in [8]. It was shown that the introduction of a periodic fast modulation into the phase of the signal beam φ_s (with no feedback) is able to modify strongly the characteristics of photorefractive 2W coupling. In particular, by choosing first a proper value of the time average $\langle\exp(i\varphi_s)\rangle$ and introducing then a small frequency detuning [linear growth of $\varphi_s(t)$] it is possible to adjust η to 1 or 0. This means that the role of the feedback consists in providing the proper fast-phase modulation of the signal beam.

In this paper we pretend to overcome the inherent defects of the previous theoretical approach, to demonstrate a variety of periodic and quasiperiodic regimes attainable at the developed stage of the nonlinear evolution (when η is near 1 or 0), and to gain direct experimental evidence of the self-oscillation behavior.

In Sec. II we formulate the basic relations for the feedback-controlled two-beam coupling, consider its experimental realization, and introduce modified feedback conditions that incorporate (in contrast to the ideal ones) inertia of the feedback loop. Experimental details are described in Sec. III. In Sec. IV we analyze the initial stage of the nonlinear development, including the effect of ideal and inertial feedback conditions and the spatial characteristics of the grating theoretically and experimentally. Section V represents an extended introduction into various operation regimes of the feedback controlled two-beam coupling. Section VI summarizes the relevant original experimental data. Discussion of the obtained results is presented in Sec. VII and conclusions are drawn in Sec. VIII.

II. BASIC RELATIONS

A. Initial equations

We suppose that two coherent light beams, the reference wave (R) and the signal wave (S), are incident onto the crystal as shown schematically in Fig. 1. These beams form a dynamic grating of the refractive index and diffract from this grating. The set of equations for such a two-beam coupling can be written in the standard dimensionless form [7,8],

$$\partial_{\xi}R=iES, \tag{1}$$

$$\partial_{\xi}S=iE^{*}R, \tag{2}$$

$$(e^{i\delta}\partial_{\tau}+1)E=e^{i\theta}R\,S^{*}. \tag{3}$$

Here ξ and τ are the dimensionless coordinate and time, R and S are the dimensionless complex amplitudes of the reference and signal beams, E is the dimensionless complex grating amplitude, θ and δ are the characteristic phases, and the asterisk stands for complex conjugation. The coordinate ξ varies from 0 to ξ_0 where ξ_0 is the dimensionless crystal thickness.

The set (1)–(3) has a broad field of applicability because it is valid for many particular microscopic models of the photorefractive nonlinearity. The specification of the introduced dimensionless parameters for the simplest models can be found in [9]. The material properties in our equations are characterized by the phases θ and δ. The first of them, θ, is of prime importance. It characterizes the type of the photorefractive response and ranges from 0 to 2π. For the so-called nonlocal (diffusion) response we have $\theta=\pm\pi/2$, whereas for the local response we should set $\theta=0$ or π. A nonzero value of the phase δ means that the rate of relaxation of the grating amplitude is a complex quantity; quite often δ is close to zero. In any case we have $|\delta|<\pi/2$.

Equations (1) and (2) describe mutual Bragg diffraction of the reference and signal beams from the grating. The total light intensity remains constant during propagation. Without loss of generality we suppose that the dimensionless total intensity $|R|^2+|S|^2=1$. Equation (3) describes recording of the grating by the light interference pattern. In the general case, the grating fringes, as well as the interference fringes, are bent. Moreover, they are changing in time and can move quite freely. Analytical solutions to Eqs. (1)–(3) can be obtained only for a restricted amount of particular and limiting cases [9].

Most experiments relevant to the subject of our studies have been performed with $LiNbO_3$:Fe crystals. Because of the importance of this case, we provide the reader with the relationships between the physical and dimensionless parameters and with the relevant numerical estimates. In this material the buildup of the grating is due to the photovoltaic charge transport and the linear electro-optic effect. We have here $|\theta|,|\delta|\ll 1$, $\xi=gx$, and $\tau\simeq t/t_d$, where x and t are the real coordinate and time, respectively, t_d is the dielectric relaxation time, $g\simeq\pi n^3 r E_{pv}/\lambda$, n the refractive index, λ the wave length, r the relevant electro-optic coefficient, and E_{pv} the photovoltaic field. Since the dielectric relaxation in $LiNbO_3$:Fe is predominantly due to photoconductivity, the time t_d is inversely proportional to the total photon flux. In experiment t_d ranges from 10^1 to 10^3 s. If the light beams are extraordinary, we have a useful numerical estimate for $\lambda=514$ nm, namely $g[\mathrm{cm}^{-1}]\simeq 2E_{pv}$ [kV/cm]. The photovoltaic field in $LiNbO_3$:Fe ranges from a few tens to $\simeq 100$ kV/cm. Therefore a crystal thickness x_0 in the order of 1 mm corresponds to a dimensionless thickness $\xi_0=gx_0$ much greater than one. For ordinary light polarization the factor g is approximately three times less than for extraordinary.

B. Fundamental amplitudes

It is important that Eqs. (1) and (2) do not include the time derivatives and that they are linear in R and S. This allows us to come to general relations characterizing the essence of the diffraction process.

Let us consider Eqs. (1) and (2) at an arbitrary time τ, taking into account that the grating amplitude E is a certain

single-valued function of the coordinate ξ. Then we can claim that these linear differential equations possess the fundamental solution $R=\mathcal{R}_r(\xi)$, $S=\mathcal{S}_r(\xi)$, meeting the boundary conditions $\mathcal{R}_r(0)=1$, $\mathcal{S}_r(0)=0$. This solution corresponds, obviously, to a testing of the spatial grating (at the moment τ) by a single beam of unit amplitude incident in the R direction, see Fig. 1. The amplitudes $\mathcal{R}_r(\xi)$ and $\mathcal{S}_r(\xi)$ are nothing else than the transmitted and diffracted parts of this testing beam.

Analogously, we introduce another fundamental solution of Eqs. (1) and (2), $R=\mathcal{R}_s(\xi)$, $S=\mathcal{S}_s(\xi)$ that meets the boundary conditions $\mathcal{R}_s(0)=0$, $\mathcal{S}_s(0)=1$ and corresponds to testing of the same grating by a single S beam of unit amplitude. Correspondingly, the fundamental amplitudes $\mathcal{R}_s(\xi)$ and $\mathcal{S}_s(\xi)$ are the diffracted and transmitted parts of this testing S beam. Further, one can check from Eqs. (1) and (2) the following important relations:

$$\mathcal{S}_s(\xi,\tau)=\mathcal{R}_r^*(\xi,\tau); \quad \mathcal{R}_s(\xi,\tau)=-\mathcal{S}_r^*(\xi,\tau). \tag{4}$$

We have retained here the argument τ to underline that these relations are valid for any time moment. Equations (4) express the physical equivalence of the beams S and R in Eqs. (1) and (2).

The diffractive properties of the grating are fully characterized by any of the above fundamental solutions. The quantity $\eta=|\mathcal{R}_s(\xi_0)|^2\equiv|\mathcal{S}_r(\xi_0)|^2$ is nothing else than the diffraction efficiency of the grating at time τ. Furthermore we have $|\mathcal{R}_r(\xi_0)|^2\equiv|\mathcal{S}_s(\xi_0)|^2=1-\eta$.

Let now $R_0=R(0,\tau)$ and $S_0=S(0,\tau)$ be the input values of the amplitudes R and S. Then the solution of Eqs. (1) and (2) is expressed by the fundamental amplitudes,

$$R=R_0\mathcal{R}_r+S_0\mathcal{R}_s, \quad S=R_0\mathcal{S}_r+S_0\mathcal{S}_s. \tag{5}$$

These relations represent R and S explicitly as sums of transmitted and diffracted components.

The dependence of the fundamental amplitudes on τ is governed by Eq. (3). It is clear from this equation that the characteristic dimensionless time of recording (buildup time) is of the order of one. A much faster change of the input amplitudes R_0 and S_0 does not affect the fundamental amplitudes. It can, however, strongly affect the output amplitudes $R(\xi_0,\tau)$ and $S(\xi_0,\tau)$ because of changing readout conditions in accordance with Eqs. (5).

Note once more that our approach sets no restrictions on the spatial dependence of the grating amplitudes, i.e., on the shape of the grating fringes.

C. Feedback equations

To formulate the feedback equations, we introduce the phase difference Φ_s between the diffracted and transmitted components of the signal beam at the output surface, $\xi=\xi_0$. According to Eqs. (5) we have

$$\Phi_s=\varphi_r+\arg[\mathcal{S}_r(\xi_0)]-\varphi_s-\arg[\mathcal{S}_s(\xi_0)], \tag{6}$$

where $\varphi_r=\arg(R_0)$ and $\varphi_s=\arg(S_0)$ are the input phases of the beams R and S. Then the initially introduced feedback equations read

$$\Phi_s=\pm\frac{\pi}{2}. \tag{7}$$

In what follows we call them the ideal feedback conditions. They define the desired value of Φ_s. A few simple relations that follow from Eq. (7) can be found in [7].

As is clear from Eq. (6), for any nonzero values of $\mathcal{S}_s(\xi_0)$ and $\mathcal{S}_r(\xi_0)$, i.e., for $\eta(1-\eta)\neq 0$, we can always fulfill the ideal feedback conditions adjusting the input phase φ_s (or φ_r). In experiment, the phase φ_s is used for adjustment. Accordingly, we assume from now on that $\varphi_r=\text{const}$; without loss of generality this constant can be set equal to zero.

In the case $\eta(1-\eta)=0$, when either the diffracted or the transmitted component of the signal beam is zero at the output surface, the introduced ideal feedback conditions make no sense. This circumstance is, as we shall see below, disastrous for the ideal feedback.

To proceed, we need to touch the question of experimental implementation of the feedback. In practice, adjustment of the phase φ_s is accomplished with the help of a modulation technique. An auxiliary (small and fast) oscillating component, $\delta\varphi_s=\psi_d\sin\omega\tau$ with $\omega\approx 10^3$ and $\psi_d\ll 1$, is introduced into the phase of the signal beam. This component does not affect the grating amplitude and serves only for initiation of the feedback loop. The introduced additional phase modulation results in the replacement of S_0 by $S_0\exp(i\psi_d\sin\omega\tau)$ in Eqs. (5). Correspondingly, the output intensity $|S(\xi_0,\tau)|^2$ acquires a high-frequency components oscillating as $\sin\omega\tau$ and $\cos 2\omega\tau$. The amplitudes of these components are

$$I_\omega=2|R_0S_0|\sqrt{\eta(1-\eta)}\psi_d\sin\Phi_s, \tag{8}$$

$$I_{2\omega}=0.5|R_0S_0|\sqrt{\eta(1-\eta)}\psi_d^2\cos\Phi_s.$$

Using $\pm I_{2\omega}$ as an error signal in an electronic feedback loop one can keep $\Phi_s\simeq\pi/2$ (or $-\pi/2$, depending on the sign of the feedback: positive or negative) till the product $\eta(1-\eta)$ becomes small.

In experiment, see also below, the error signal initiates a displacement of a mirror. The essence of the feedback controlled motion of the mirror is that its velocity is proportional to $I_{2\omega}$. This leads to the following phenomenological relation for the time derivative $\dot{\varphi}_s$,

$$\dot{\varphi}_s=\mp\frac{1}{\tau_f}|R_0S_0|\sqrt{\eta(1-\eta)}\cos\Phi_s, \tag{9}$$

where τ_f is the response time of the feedback loop. The introduced characteristic time incorporates the amplification and the integration of the error signal, as well as the piezodriver characteristics. This time has to be very small, $\tau_f\ll 1$, to make the feedback operative. Note that the factor $|R_0S_0|$ entering Eq. (9) is half the contrast of the light interference pattern at the input.

Let us assume that the value of $\sqrt{\eta(1-\eta)}$ is far from zero and that the diffractive characteristics of the grating, namely η and $\arg[\mathcal{S}_r(\xi_0)\mathcal{S}_s^*(\xi_0)]$, vary slowly in the scale of τ_f. Then, as follows from Eq. (9), the phase φ_s approaches quickly (within a time period comparable with τ_f) the value $\varphi_s = \arg[\mathcal{S}_r(\xi_0)\mathcal{S}_s^*(\xi_0)] \mp \pi/2$ that guarantees that $\Phi_s \simeq \pm\pi/2$. In such a way, the signs $\mp$ in Eq. (9) correspond to the feedback conditions $\Phi_s = \pm\pi/2$.

In contrast to the ideal feedback conditions (7), the phenomenological equations (9) take the inertia of the feedback into account. This inertia becomes especially important when the product $\eta(1-\eta)$ approaches zero. The phase φ_s loses here the ability to follow the desired value $\arg[\mathcal{S}_r(\xi_0)\mathcal{S}_s^*(\xi_0)] \mp \pi/2$ and consequently the phase Φ_s can deflect strongly from its ideal value. According to Eq. (9), the maxima and minima of the input phase φ_s take place when the product $\sqrt{\eta(1-\eta)}\cos\Phi_s$ becomes zero.

III. EXPERIMENTAL DETAILS

The main features of our experimental setup, which are similar to those described in [4–6], can be described with the help of Fig. 1. Two extraordinary polarized coherent light beams impinge upon a sample of lithium niobate in the plane containing its optical axis. The feedback loop includes a standard lock-in amplifier (Stanford Research model SR 830 DSP), an integrator, and a piezo-driver (Physik Instrumente model P840.10) with the maximum displacement of 15 μm. The piezomounted mirror, placed into one of two interferometer lags, introduces a small-amplitude ($\psi_d \simeq 0.1$ rad) fast ($\omega \simeq 500\,\pi$ rad/s) sinusoidal phase modulation in the signal beam.

The signal from the photodetector PD is sent to the input of the lock-in amplifier tuned to extract the error signal $I_{2\omega}$. A nonzero error signal from the lock-in amplifier is accumulated in the analog integrator feeding the piezomounted mirror. This results in a mirror motion with a velocity proportional to $I_{2\omega}$ within a dynamic range from $\approx 10^{-4}$ to ≈ 10 Hz. The output of the integrator is automatically reset (to zero/ground) when the driving voltage reaches a certain limiting value defined by the piezodriver specifications.

In our experiments we have used a 0.35-mm-thick sample of $LiNbO_3$:Fe. Its 4×5 mm^2 input/output faces are parallel to the optical axis. The crystal has a congruent composition, contains 0.1 wt% of Fe_2O_3 and is grown in an oxidizing atmosphere (air). This is why the photoconductivity of our sample is relatively low [10] and the photovoltaic field is very large, $E_{pv} \approx 100$ kV/cm at $\lambda = 532$ nm.

The operation of the feedback loop has been studied at two recording wavelengths. Two lasers were used: A 100-mW frequency-doubled YAG:Nd^{3+} (where YAG is yttrium aluminum garnet) laser ($\lambda = 532$ nm) and a 50-mW He-Ne laser ($\lambda = 633$ nm). With the He-Ne laser we use unexpanded light beams ($1/e^2$ intensity diameter $d \simeq 4$ mm), while the YAG:Nd^{3+} laser beam was slightly ($d \simeq 5$ mm) expanded.

The angle between the incident light beams was $\simeq 12°$. At 532 nm this corresponds to a grating spacing of $\simeq 2.2$ μm and to a diffusion field of $E_D \simeq 650$ V/cm. At 633 nm the corresponding parameters are $\simeq 3\,\mu$m and $\simeq 540$ V/cm. In both cases the diffusion field is much smaller than the photovoltaic field.

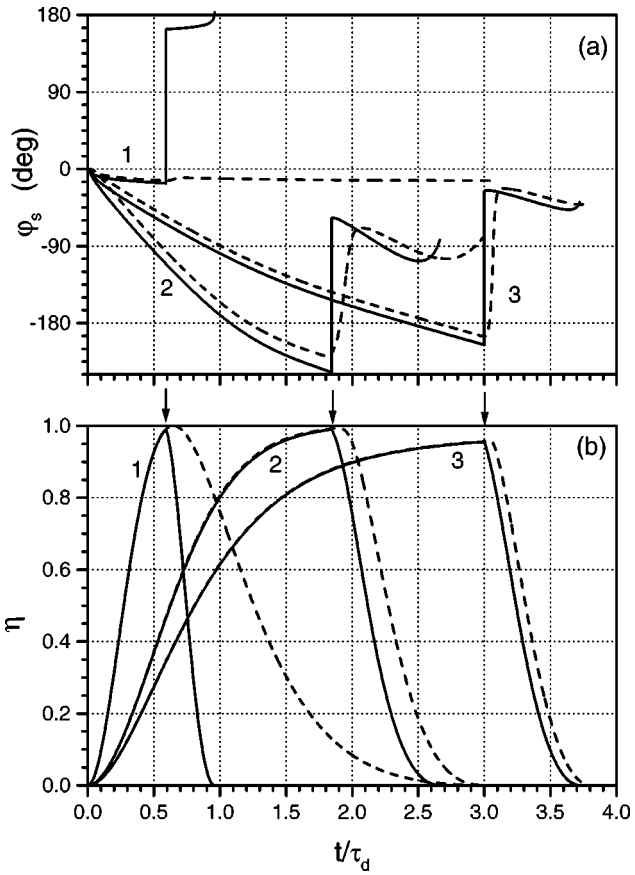

FIG. 2. Feedback-controlled dependences $\eta(\tau)$ and $\varphi_s(\tau)$. The solid curves correspond to the ideal feedback and the dashed ones to the inertial feedback equations. The curves 1, 2, and 3 are plotted for the pairs of parameters $\xi_0 = 6.6$, $\beta = 1$; $\xi_0 = 6.6$, $\beta = 15$; and $\xi_0 = 4$, $\beta = 6$; respectively. The arrows indicate the time of switching from $\pi/2$ to $-\pi/2$ feedback conditions.

IV. INITIAL STAGE OF DEVELOPMENT

An exciting feature of the ideal feedback $\Phi_s = \pi/2$ is that it always tends to increase the diffractivity of the grating during recording. This feature has no analogs among the photorefractive schemes. If the crystal is thick enough, $\xi_0 > \xi_0^{th}$, the diffraction efficiency $\eta(t)$ approaches its ultimate value $\eta = 1$ within a finite time. In the case $\delta = 0$ and $\theta = 0$ the threshold thickness ξ_0^{th} is given by [7]

$$\xi_0^{th} = \pi + \frac{1}{\pi}\ln^2\beta, \tag{10}$$

where $\beta = |S_0|^2/|R_0|^2$ is the input beam ratio.

Figure 2 shows typical examples of the feedback-controlled behavior for η and φ_s. The initial solid sections of the curves (up to the points marked by the arrows) are obtained for the ideal feedback $\Phi_s = \pi/2$ and the dashed ini-

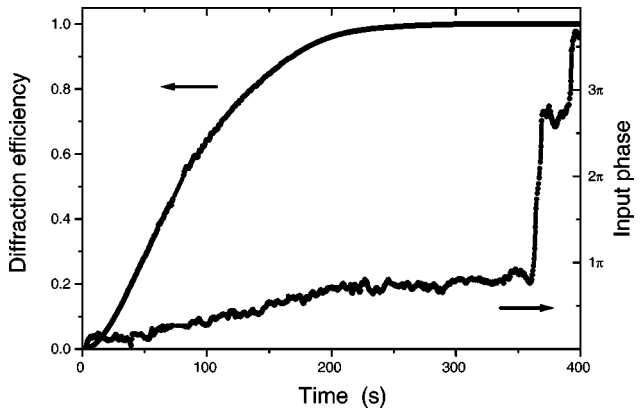

FIG. 3. Experimental dependences $\eta(t)$ and $\varphi_s(t)$ for $\beta=9$ and the $\pi/2$ feedback.

tial sections are plotted for the corresponding inertial feedback conditions given by Eq. (9). For the characteristic phases θ and δ we have chosen the values 6.8×10^{-2} and 6.7×10^{-3}, respectively, representative for $LiNbO_3$:Fe crystals. For $\xi_0<\xi_0^{th}$ the efficiency η approaches its steady-state value $\simeq0.98$ monotonously whereas the phase φ_s tends to a linear dependence, $\varphi_s=\Omega_s\tau$, see the curves 3. These limiting characteristics correspond to the steady-state solution of Eqs. (1)–(3) with the frequency detuning Ω_s maximizing η for chosen ξ_0 and β. This solution can easily be found analytically. Since $\Omega_s\neq0$, the grating is moving in steady state.

For $\xi_0>\xi_0^{th}$, the diffraction efficiency approaches unity monotonously within a finite time, see the curves 1 and 2. The characteristic dimensionless time of this stage is greater than or comparable with 1. The smaller the distance $\xi_0-\xi_0^{th}$, the longer is this time. The phase φ_s demonstrates a regular behavior and approaches a certain limiting value when η tends to 1. The difference between the solid and dashed curves is not large for φ_s and nearly nondistinguishable for η at the initial stage. This difference increases, as expected, when η approaches 1. The shorter the characteristic time τ_f, the smaller the difference between the solid and dashed curves.

The sections of the solid and dashed curves 1, 2, and 3, in Fig. 2 that start from the time moment indicated by the arrows show what happens when we switch from the $\pi/2$ to the $-\pi/2$ feedback conditions. One sees that the diffraction efficiency reaches zero within a finite time. For the ideal feedback, the phase φ_s experiences a 180° jump at the moment of switching whereas it changes continuously for the inertial feedback conditions. The difference between the effects of the ideal and inertial feedback is clearly seen at this stage. The longer the time spent in the close vicinity of $\eta=1$, the stronger this difference.

Figure 3 gives a representative example of the experimental dependences of $\eta(t)$ and $\varphi_s(t)$ for the initial stage and the $\pi/2$ feedback condition. The photorefractive response time is here about 200 s and the pump ratio $\beta=9$. One sees that in agreement with theory the diffraction efficiency monotinously approaches 1 whereas the input phase φ_s gradually increases. The initial stage ends up at $t\approx350$ s when the phase φ_s first experiences a jump; the value of η is

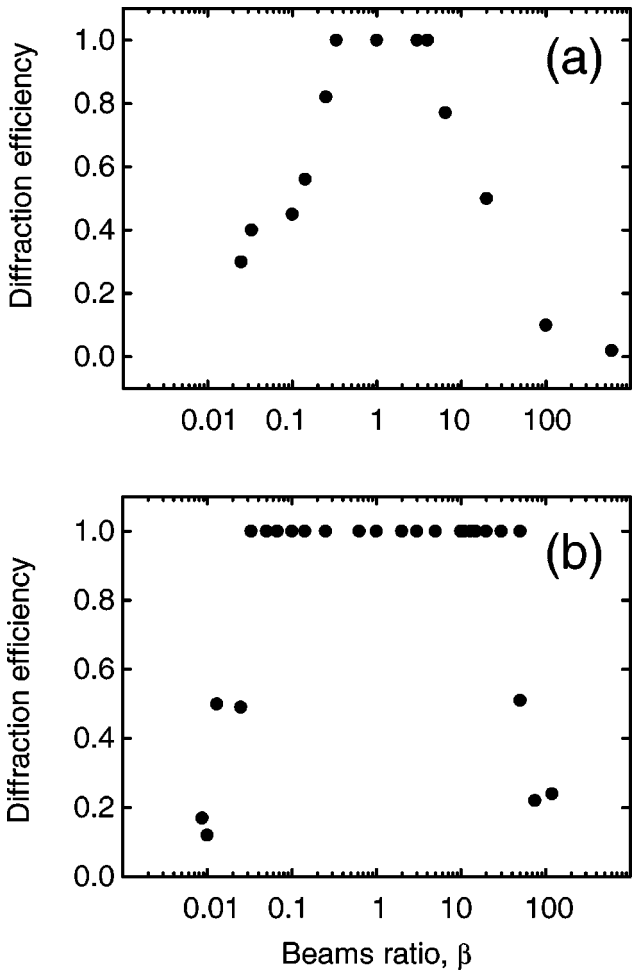

FIG. 4. The saturated experimental value of η versus pump ratio at 633 nm (a) and 532 nm (b).

almost saturated at this time. Figure 4 shows the dependence of the saturated value of η on β for red ($\lambda=633$ nm) and green (532 nm) light, which corresponds to two different values of the effective crystal thickness ξ_0. It is clearly seen that the saturated value $\eta\simeq1$ can be obtained only within a restricted interval of β. The larger ξ_0, the wider is this interval. This feature is also in full agreement with theoretical predictions.

Figure 5 demonstrates the spatial characteristics of the grating and of the light interference pattern at the time moments indicated by the arrows in Fig. 2. Ideal and inertial feedback give here essentially the same result. We see that the grating and light fringes are generally bent and they do not follow each other. The absolute value of the grating amplitude changes considerably across the crystal. A nearly complete energy exchange between the light beams occurs at the output for $\beta\neq1$. We can conclude from these data that the language of plain (uniform) gratings (very useful for intuitive and qualitative considerations) cannot generally be applied to the analysis of feedback controlled beam coupling. This circumstance creates a serious problem for the understanding of this phenomenon.

We know only one case, charcterized by $\delta=0$, $\theta=0$, and $\beta=1$, without an effect of the spatial nonuniformity. Here

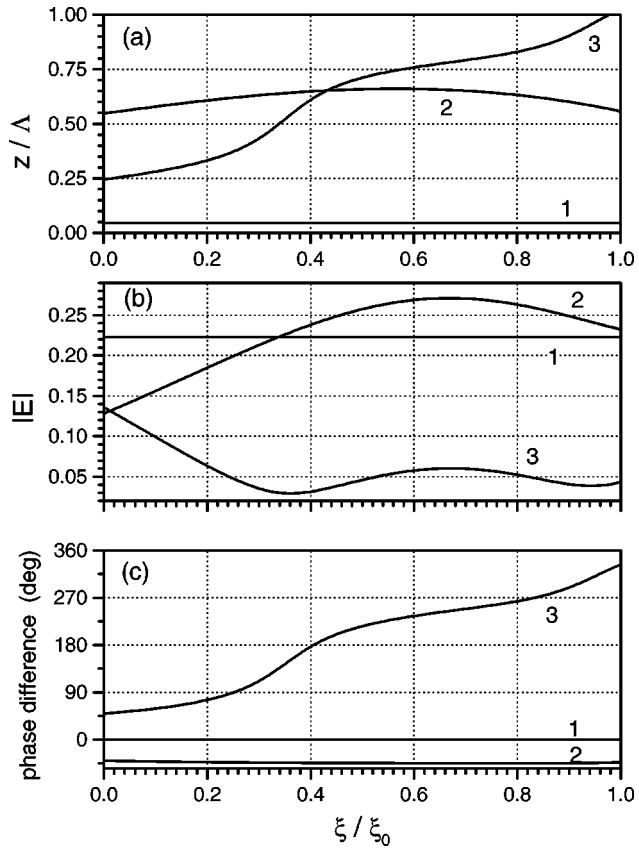

FIG. 5. Spatial characteristics of the feedback-controlled two-beam coupling: (a) The form of the grating fringes, (b) the spatial dependence of the absolute value of the grating amplitude, (c) the spatial dependence of the phase difference $\arg E - \arg(RS^*)$ between the grating and light fringes. The graphs 1, 2, and 3 correspond here to the solid curves 1, 2, and 3 in Fig. 2.

one can check directly that the set (1)–(3) exhibits the following spatio-temporal solution:

$$R=\frac{1}{\sqrt{2}}e^{i[\varphi_r(0)+|E|\xi]}, \quad S=\frac{1}{\sqrt{2}}e^{i[\varphi_s(0)+|E|\xi]},$$

$$E=\frac{1}{2}(1-e^{-\tau})e^{i(\varphi_r-\varphi_s)}. \tag{11}$$

Correspondingly, we have

$$\mathcal{S}_s=\cos(|E|\xi), \quad \mathcal{S}_r=ie^{i(\varphi_r-\varphi_s)}\sin(|E|\xi) \tag{12}$$

for the fundamental solutions and

$$\eta=\sin^2[(1-e^{-\tau})\xi_0/2] \tag{13}$$

for the diffraction efficiency.

It is easy to see that in the regions where $\sin[(1-e^{-\tau})\xi_0]>0$ we have $\Phi_s=\pi/2$ whereas in the regions where $\sin[(1-e^{-\tau})\xi_0]<0$ one obtains $\Phi_s=-\pi/2$. Equations (11) show no energy exchange between the light beams, no input phase changes, $\varphi_s(t)=\varphi_s(0)$, $\varphi_r(t)=\varphi_r(0)$, no bending and tilting of the grating fringes, only some time-dependent tilt of the light interference fringes.

Let the thickness ξ_0 be smaller than $\xi_{th}(\beta=1)=\pi$. Then for $\tau>0$ when the ideal $\pi/2$ feedback conditions are fulfilled and the efficiency $\eta(\tau)$ increases monotonously from 0 to its limiting value $\eta(\infty)=\sin^2(\xi_0/2)<1$. If $\xi_0>\pi$, the efficiency approaches unity within a finite time remaining under the control of the $\pi/2$ feedback. This behavior is in full agreement with the above numerical results, see Fig. 2. At time moment when $\eta(\tau)$ turns to 1 the ideal feedback condition $\Phi_s=\pi/2$ fails and it cannot define the further temporal development of the system.

Now we suppose that $\xi_0>\pi$ and $\sin[(1-e^{-\tau})\xi_0]<0$, which corresponds to the ideal $-\pi/2$ feedback. Here we have a monotonous decrease of η. If additionally $\xi_0>2\xi_0^{th}=2\pi$, this decrease ends up with $\eta=0$ where the ideal feedback condition $\Phi_s=-\pi/2$ also ceases to define the further development. In such a way, our analytical example confirms once more that the ideal $+\pi/2$ and $-\pi/2$ feedbacks increase and decrease η without any inertia and that they can control the system only during restricted time intervals.

Generalization of the above analytical result for $\beta\neq 1$ runs into considerable problems because of the nonuniformity of the spatial grating. Our confidence that the inequality $\dot{\eta}\geqslant 0$ for $\Phi_s=\pi/2$ and the inequality $\dot{\eta}\leqslant 0$ for $\Phi_s=-\pi/2$ are always fulfilled is based mostly on the large amount of our numerical calculations.

V. WHAT IS BEYOND $\eta=1$?

A. General remarks

We conclude from the results of the previous section that the ideal $\pi/2$ feedback leads to a state with $\eta=1$ where the feedback condition $\Phi_s=\pi/2$ fails. Hence the corresponding mathematical model remains correct only within a restricted time interval and we cannot describe the system beyond it. Physically, this means that the ideal feedback conditions should be modified to overcome their inherent defect.

One of the simplest modifications is as follows. We define $\varphi_s(t)$ from the ideal feedback condition $\Phi_s=\pi/2$ only for $\eta<\eta_c$, where η_c is a certain critical value, such that $0<1-\eta_c\ll 1$. As soon as η becomes larger than η_c, we keep the phase φ_s equal to its last feedback controlled value. As soon as η becomes (after some evolution) less or equal than η_c, the feedback $\Phi_s=\pi/2$ starts to operate again. This modified model is mathematically correct. It allows us to describe the whole evolution of the system and to understand the properties of the ideal feedback better. Actually, it accounts for the possibility that the accuracy of the control of φ_s goes down when η approaches 1 and the error signal can finally be superimposed by noise. The region where $\eta>\eta_c$ is here passive for the ideal feedback so that we shall refer to this model as the passive-region model.

The inertial feedback equations (9) promise to overcome the inherent defect of the ideal feedback in a more realistic way. As long as η is sufficiently far from 1, there is not much difference from the ideal feedback. At the same time,

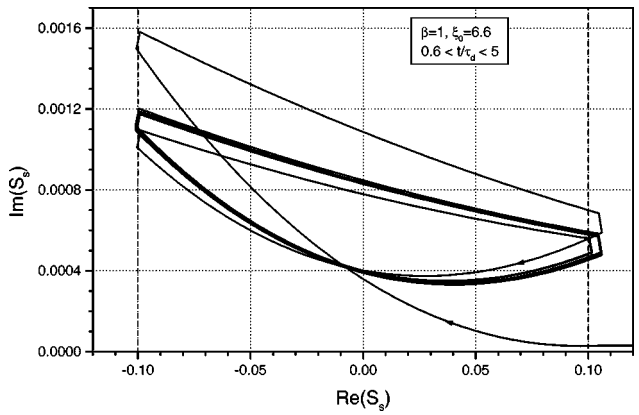

FIG. 6. Trajectory of $\mathcal{S}_s(\xi_0,\tau)$ in the complex plane for $\xi_0=6.6$, $\beta=1$, and $0.6\leqslant\tau\leqslant 5$.

in the vicinity for $\eta(1-\eta)=$ the real features of any experimental setup are reflected. One will expect that the inertial feedback can operate permanently.

In the following subsections we present the results obtained numerically for the passive-region model and for the inertial feedback. Our main concerns are: What is the behavior of the input phase φ_s in the long-time scale? What happens with the phase difference Φ_s between the diffracted and transmitted components of the signal beam? How small can the distance $1-\eta$ become at the final state? What are the main requirements on the characteristics of the feedback loop? And, finally, what kind of predictions can be made for experiment?

An element of our consideration will be the representation of the fundamental amplitudes by trajectories in the complex plane. This representation is similar to those used to describe nonlinear dynamic systems [11,12]. It gives a great deal of additional information on the behavior of our system as compared with the data for $\eta(t)$ and $\varphi_s(t)$. In the subsequent calculations we use again the values of the characteristic phases representative for $LiNbO_3$, $\theta=6.8\times10^{-2}$ and $\delta=6.7\times10^{-3}$.

B. The passive-region model

Figure 6 shows a trajectory $\mathcal{S}_s(\xi_0,\tau)$ for the input beam ratio $\beta=1$ and the crystal thickness $\xi_0=6.6$. For the critical value of the diffraction efficiency we have taken here $\eta_c=0.99$. The dashed curve marks the boundary of the passive region that is inside a circle of radius $|\mathcal{S}_s(\xi_0)|\equiv\sqrt{1-\eta_c}=0.1$ (note the very different scales of the coordinate axes). One sees that the trajectory enters the passive region almost horizontally in accordance with the analytical expression (12) for $\mathcal{S}_s$. Further events occur indeed inside this region. A small fraction of the time spent outside is due to our discretization procedure. A decrease of the time step results in a reduction of this fraction. Thus the ideal feedback shows no inertia: as soon as it is on, it pushes the trajectory back into the passive region so that the system develops freely almost all the time. After several ''reflections'' from the boundary the trajectory approaches a limit cycle (attractor). The further behavior of $\mathcal{S}_s(\xi_0,\tau)$ is nearly periodic with a period considerably less than 1. This fast periodic motion of $\mathcal{S}_s(\xi_0,\tau)$ in the passive region is accompanied by a slow motion of the amplitude $\mathcal{S}_r(\xi_0,\tau)$ (superimposed by small and fast oscillations) near the the unit circle $|\mathcal{S}_r|=1$.

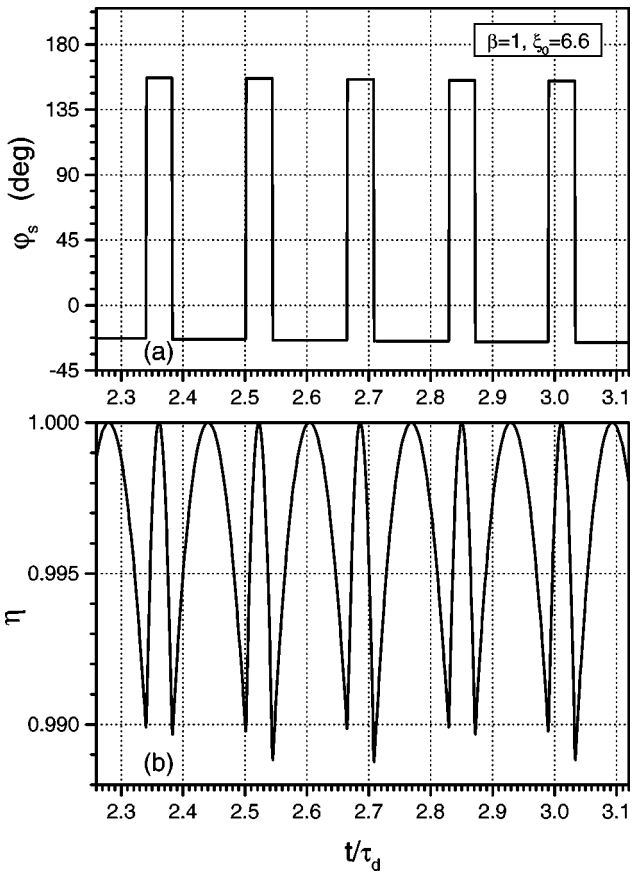

FIG. 7. Dependences $\varphi_s(\tau)$ and $\eta(\tau)$ for $\xi_0=6.6$, $\beta=1$, and $2.26\leqslant\tau\leqslant3.12$.

Figure 7 shows the dependences $\varphi_s(t)$ and $\eta(t)$ for the limit cycle. The reflections of the trajectory from the left and right sides of the boundary are accompanied by jumps of the input phase of almost π. These jumps are indeed due to the fact that the feedback finds the right value of the phase φ_s as soon as the trajectory crosses the boundary of the passive region. It is interesting that the times necessary to cross this region back and forth are quite different and also that the periodic phase dependence is accompagnied by a small negative slope, i.e., the function $\varphi_s(t)$ includes also a linear component $\Omega_s\tau$ with $\Omega_s<0$. It is known that such a component is necessary to maintain $\eta\simeq1$ in the presence of fast phase modulation [8]. In the case $\beta=1$ this component is due to the nonzero value of θ. When the trajectory in Fig. 6 enters the passive region, the maximum diffraction efficiency is already very close to unity and this same maximum value occurs each time half-way when crossing the passive region.

This character of the feedback operation persists when the beam ratio β ranges from 1 to $\simeq22$. The main quantitative changes are a gradual shift of the position of the attractor towards the right-upper part of the passive region, a certain increase of the oscillation period, and a noticeable increase of the average slope (an increase of $|\Omega_s|$).

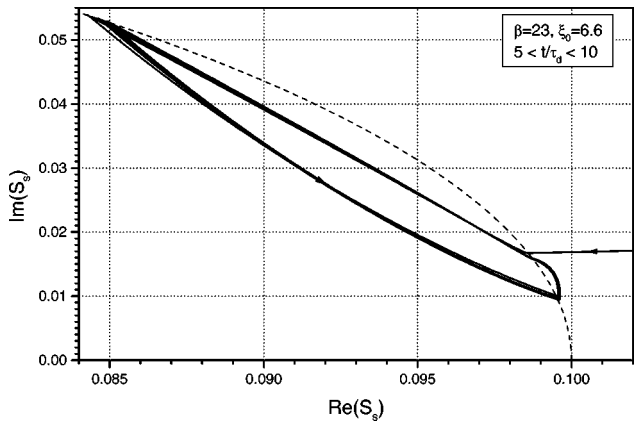

FIG. 8. Trajectory of $\mathcal{S}_s(\xi_0,\tau)$ for $\beta=23$, $\xi_0=6.6$, and $5\leqslant\tau\leqslant10$.

A qualitative feature in the behavior of the system appears when the beam ratio approaches its threshold value from below, which is $\beta^{th}\simeq23.5$ for the given crystal parameters. The phase portrait for $\beta=23$ is shown in Fig. 8. The trajectory enters the passive region nearly horizontally and not far from the real axis and becomes then nearly closed. The characteristic feature of this quasiattractor is that it lies essentially outside the passive region. This part does not disappear with decreasing time steps. In other words, the ideal feedback demonstrates in this limit some noticeable inertia.

Figure 9 gives the corresponding dependences of η and φ_s. One sees that the system spends a considerable part of the time outside the passive region. The phase φ_s experiences now only a small jump when the trajectory goes outwards that is not sufficient to push the trajectory back into the passive region. The presence of a considerable average slope (a large $|\Omega_s|$) is also clearly indicated in Fig. 9.

Starting from 1, a decrease of β shifts the attractor nearly symmetrically towards the left-lower section of the passive region. The sign of the average slope is changing from negative to positive.

On the basis of the results presented above it is not difficult to anticipate what happens with the system if, instead of the introduction of a critical value of η, we add a small noise component to the error signal. Until the distance $1-\eta$ is sufficiently small, the effect of noise is not very important and the trajectory $\mathcal{S}_s(\xi_0,\tau)$ will approach zero. As soon as it is near enough to zero, the noise governs the trajectory and it walks randomly inside an effective passive region. When this random trajectory withdraws too far away from zero the error signal pushes it back into the passive region. Note finally that in our experiments we did not see any sign of the behavior predicted by the passive-region model.

C. Regimes of the inertial feedback model

As our simulations show, the inertial equations (9) allow the feedback to operate permanently. The feedback-controlled system exhibits here a great variety of regimes, mostly due to the occurrence of the second characteristic time, τ_f. What is presented below is an attempt to outline the most prominent features of the nonlinear behavior of the

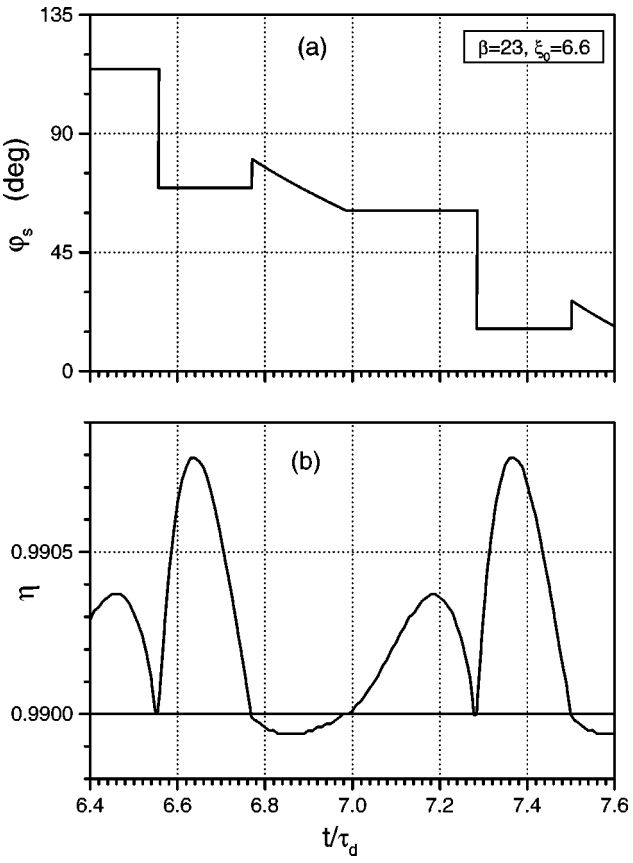

FIG. 9. Dependences $\varphi_s(\tau)$ and $\eta(\tau)$ for $\xi_0=6.6$, $\beta=23$, and $6.4\leqslant\tau\leqslant7.6$.

system for moderately thick crystals, whose dimensionless thickness ξ_0 is not much greater than the threshold thickness ξ_0^{th}.

It is useful to start with the case of an intermediate beam ratio β (between 1 and $\beta^{th}\simeq\exp[\sqrt{\pi(\xi_0^{th}-\pi)}]$, see Eq. (10)). Figure 10 shows the time dependences of φ_s, η, and Φ_s for $\tau_f=10^{-3}$, $\xi_0=6.6$, and $\beta=4$. After a relatively short initial stage, $0<\tau\lesssim1$, the phase φ_s shows a quite regular but non periodic behavior. It is characterized by almost periodic steps upwards, each of them as large as $\simeq340°$. The time distance between the time steps is $\simeq0.35$. These steps produce a considerable positive average slope of the dependence $\varphi_s(\tau)$.

The input phase steps are accompanied by apparently periodic oscillations of the diffraction efficiency in the vicinity of 1 with a clear fine structure. The period of these oscillations ($\simeq0.35$) is apparently the same as the distance between the phase steps. The phase Φ_s, responsible for the error signal, remains only during the initial stage close to $\pi/2$; its further behavior is characterized by strongly quasiperiodic and strongly nonharmonic oscillations. This has nothing to do with the behavior prescribed by the ideal feedback conditions. A further increase of τ makes the phase steps of φ_s and the periodic oscillations of η and Φ_s even more ideal. Note that the sharp peaks and dips of $\Phi_s(\tau)$ do not strongly affect the variables φ_s and η which show a rather smooth temporal behavior.

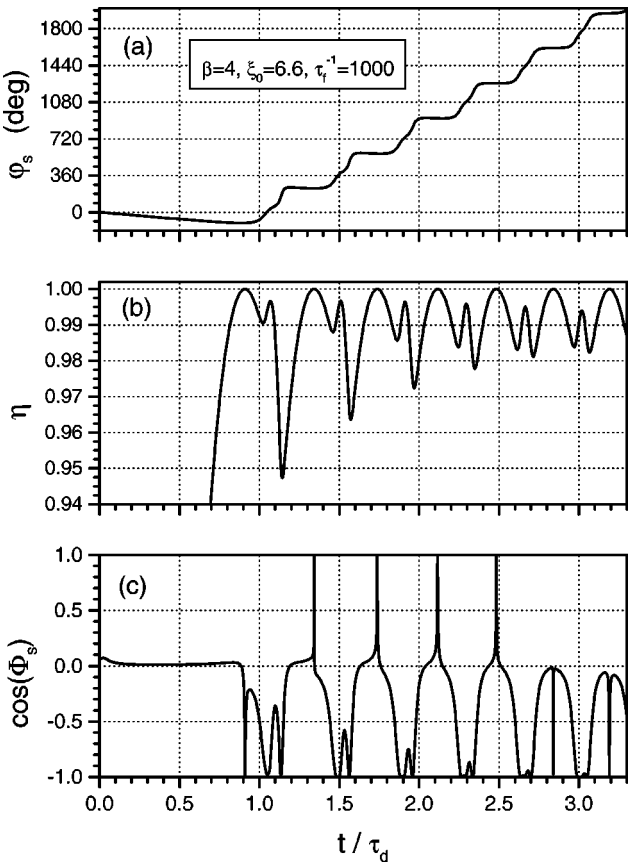

FIG. 10. Dependences $\varphi_s(\tau)$, $\eta(\tau)$, and $\Phi_s(\tau)$ for $\xi_0=6.6$, $\beta=4$, and $0\leqslant\tau\leqslant3.3$.

The solid closed curve in Fig. 11(a) exhibits the trajectory $\mathcal{S}_s(\xi_0,\tau)$ for $6\leqslant\tau\leqslant8$. During that time about seven revolutions of this trajectory occur. This shows clearly that the point $\mathrm{Re}\,\mathcal{S}_s(\xi_0,\tau)$, $\mathrm{Im}\,\mathcal{S}_s(\xi_0,\tau)$ moves along a limit cycle (an attractor). This motion is clockwise and strictly periodic in time, its period, $T\simeq0.354$, corresponds to the period of $\eta(\tau)$ and $\Phi_s(\tau)$ and to the the duration of one step of $\varphi_s(t)$, see Fig. 10. The origin, $\mathcal{S}_s=0$, lies inside the limit cycle but very close to it. This is why the peaks and dips of $\Phi_s(\tau)$ in Fig. 10 are so sharp. Some tilt of the attractor is due to a nonzero value of the characteristic phase θ. The dashed curve in Fig. 11(a) is the trajectory for $1\leqslant\tau\leqslant3$; it shows the character of the transient process. While $\mathcal{S}_s(\xi_0,\tau)$ moves along the attractor, $\mathcal{S}_r(\xi_0,\tau)$ moves with small and constant angular velocity along the unit circle, $|\mathcal{S}_r|\simeq1$. This motion is superimposed by fast periodic oscillations of the above period T.

At this point it is reasonable to ask oneself how it is possible to combine the periodic behavior of $\mathcal{S}_s$ and $\cos(\Phi_s)$ with the nonperiodic behavior of $\mathcal{S}_r$ and φ_s, keeping in mind that all these variables enter the feedback equation (9). To clarify this important point, we represent φ_s and $\mathcal{S}_r$ as

$$\varphi_s=\varphi_s^p+\Omega_s\tau,\quad \mathcal{S}_r=\mathcal{S}_r^p\exp(-i\Omega_r\tau), \tag{14}$$

where φ_s^p and $\mathcal{S}_r^p$ are T-periodic variables with average value 0, Ω_s is the frequency detuning for the signal beam, and Ω_r

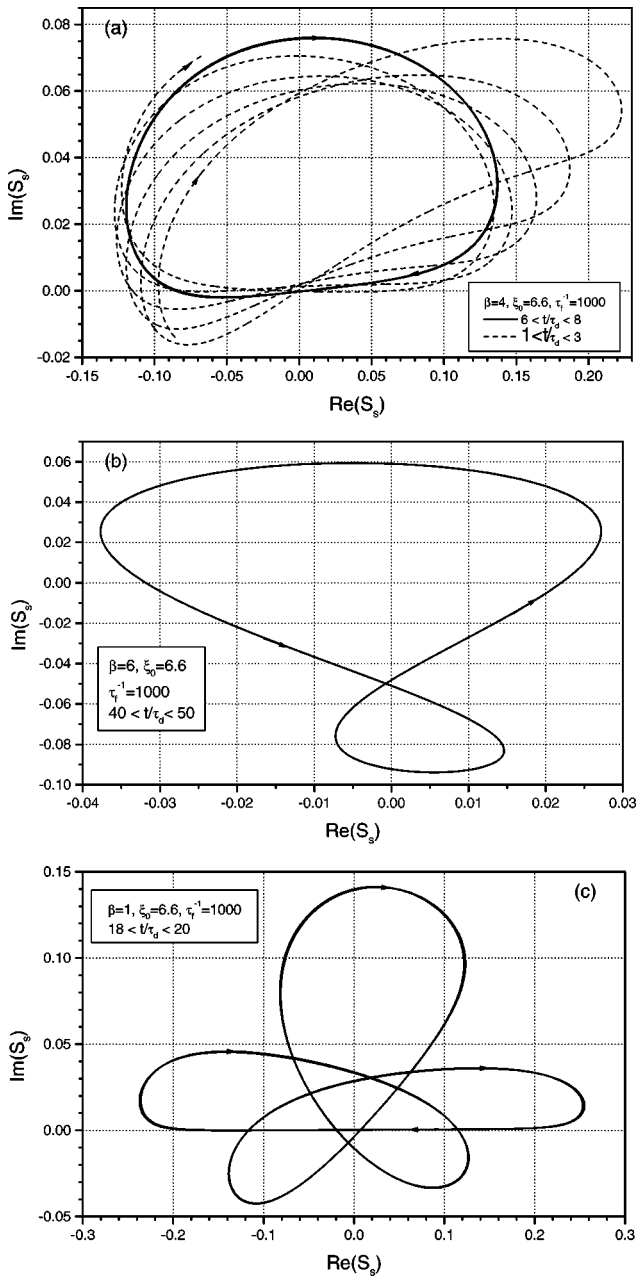

FIG. 11. (a) The orbit of $\mathcal{S}_s(\xi_0,\tau)$ for $\xi_0=6.6$ and $\beta=4$; the solid part corresponds to $6\leqslant\tau\leqslant8$ and the dashed one to $1\leqslant\tau\leqslant3$. (b) The orbit of $\mathcal{S}_s(\xi_0,\tau)$ for $\xi_0=6.6$ and $\beta=6$. (c) The orbit of $\mathcal{S}_s(\xi_0,\tau)$ for $\xi_0=6.6$ and $\beta=1$.

is the average angular velocity for the amplitude $\mathcal{S}_r$. Then the only possibility to meet Eq. (9) is to assume that

$$(\Omega_s+\Omega_r)T=2\pi N, \tag{15}$$

where $N=0,\pm1,\pm2,\ldots$. The number N depends on the attractor topology and may be called ''effective charge.'' For the above attractor $N=1$.

The frequency detuning Ω_s [the average slope of $\varphi_s(\tau)$] is an important observable characteristic of the feedback coupling. As follows from Eq. (9), it obeys the relation

$$\Omega = -\tau_f^{-1}|R_0 S_0|\langle\sqrt{\eta(1-\eta)}\cos\Phi_s\rangle, \qquad (16)$$

where the angular bracket means the average over a period. In such a way, we have expressed Ω_s by τ_f and by the characteristics of the fast oscillations. Note that Ω_s is not directly concected with the rotation rate for the amplitude $\mathcal{S}_s$. Our numerical calculations have proven the correctness of Eq. (16).

We see that our representation has revealed nontrivial features of the periodic and transient behavior of our system. At the same time we should be aware that this representation is not complete because it does not touch on the coordinate (z) dependences of the amplitudes.

A surprising feature is the relatively long period of the oscillations, $T \simeq 0.354$. Caused by the inertial feedback, this period is not much shorter than the photorefractive response time (unity in our dimensionless notation) and much longer than the feedback response time, $\tau_f = 10^{-3}$. To investigate the dependence $T(\tau_f)$, we have performed the following numerical experiment: Starting from $\tau = 12$ (when the periodic state with $\beta = 4$ is already achieved) we decreased τ_f from 10^{-3} to 4×10^{-5} with a very small rate (during the time interval 120) causing very slow (adiabatic) changes of the characteristics of the periodic solution. During this procedure, the attractor decreased in size preserving approximately the same bagel-like form as in Fig. 11(a). The period of the fast oscillations, T, also decreased with decreasing τ_f as shown by the dashed line in Fig. 12(a). Another interesting question that can be answered within our adiabatic procedure is how the average $\langle 1-\eta\rangle$ over a period of T depends on τ_f. The corresponding dependence is shown by the dashed line in Fig. 12(b).

With good accuracy, both the dependences, $T(\tau_f)$ and $\langle 1-\eta\rangle(\tau_f)$, can be approximated by the relations

$$T = C_T\sqrt{\tau_f/|R_0 S_0|}, \quad \langle 1-\eta\rangle = C_\eta \tau_f/|S_0 R_0|, \qquad (17)$$

with $C_T \simeq 7$ and $C_\eta \simeq 3.3$. These dependences are fully compatible with the structure of Eq. (9). They show, in particular, that the fast oscillations of the input phase φ_s remain strong (comparable with 2π) even when $\tau_f \to 0$. The proportionality constants C_T and C_η vary for different attractors and depend on the beam ratio β, which is demonstrated in Fig. 12.

As our simulations show, the replacement $\beta = 4$ by $\beta = 1/4$ results, roughly speaking, in the inversion of the orbit about the origin. Correspondingly, this changes the sign of the general slope of $\varphi_s(t)$ and the sign of the ''effective charge'' N.

Next we focus our attention on the case $\beta = 6$ keeping the other parameters the same. Figure 11(b) shows the corresponding attractor. It consists of two loops and the trajectory moves around zero in counter clockwise direction. The size of this attractor is considerably smaller than that of the attractor in Fig. 11(a). The origin is here in the central part of the orbit. Again the trajectory performs again only one revolution around the origin during the period T. It is remarkable that the trajectory comes close to the limit cycle only for $\tau \approx 20$, which is much longer than for the case $\beta = 4$. An adiabatic decrease of τ_f results in a gradual decrease of the size of the attractor without any remarkable change of its form. The ''effective charge'' of this attractor is zero that means that $\Omega_s = -\Omega_r$ in Eq. (15).

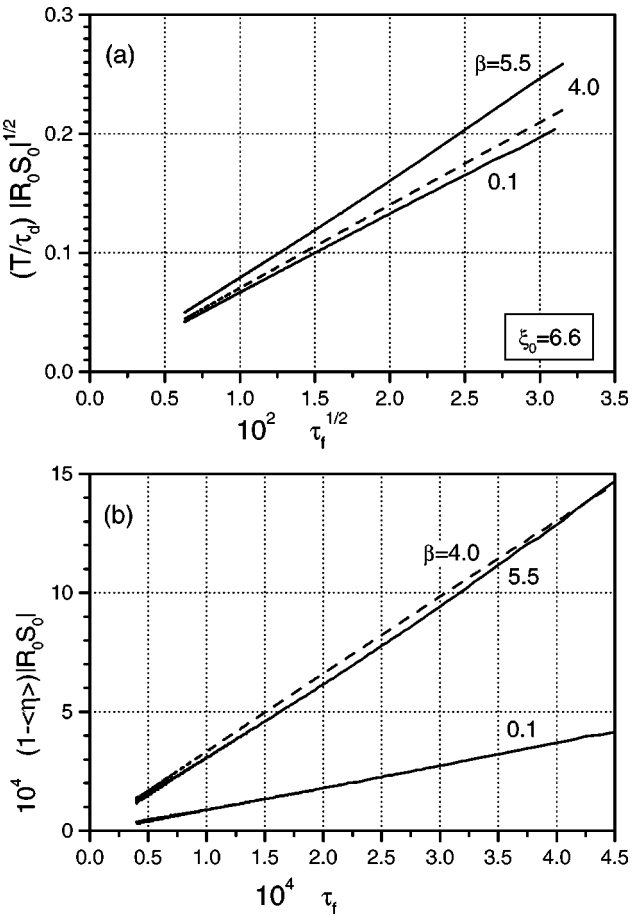

FIG. 12. Dependences $T(\sqrt{\tau_f})$ and $\langle 1-\eta\rangle(\tau_f)$ for adiabatically decreasing τ_f, $\xi_0 = 6.6$, and three different values of β.

Figure 13 gives the corresponding time dependences of φ_s and η for $0 \leqslant \tau \leqslant 10$. The average slope of the phase is now negative, it corresponds to $\Omega_s \simeq -0.924$ that is much less than for the case $\beta = 4$, compare Fig. 10. This feature is favorable for experiment because it requires less resets of the piezodriver. The fine structure (oscillations) on the graph for φ_s is strongly different from the steplike behavior in Fig. 10. It is remarkable that a quite regular phase behavior (a nearly constant slope and nearly periodic oscillations) appears as soon as η passes its first maximum in spite of the fact that the behavior of the trajectory is apparently irregular at this stage. Further development results in a rather quick regularization of the oscillations of φ_s, and η. The period of the oscillations, $T \simeq 0.33$, and the dependences of T and $\langle 1-\eta\rangle$ on τ_f are not much different from the case $\beta = 4$. The transformation $\beta \to \beta^{-1}$ gives qualitatively the same result as in the previous case.

Now we consider the case of equal input intensities, $\beta = 1$. Here the temporal development of $\mathcal{S}_s$ ends up by attraction to the limit cycle shown in Fig. 11(c). The full period corresponds here to three revolutions around zero. This leads to a period tripling of $\varphi_s(\tau)$, $\eta(\tau)$, and other variables, see

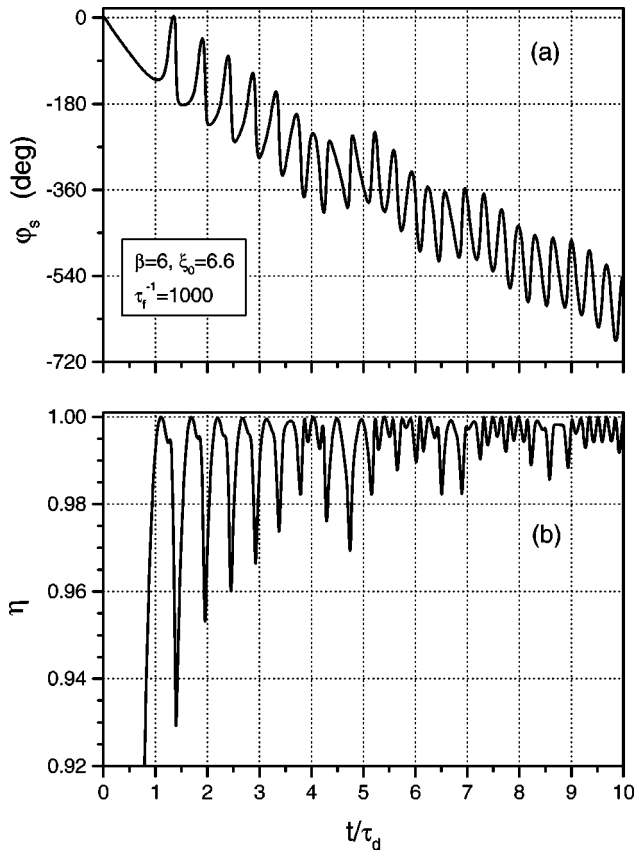

FIG. 13. Dependences $\varphi_s(\tau)$ and $\eta(\tau)$ for $\xi_0=6.6$ and $\beta=6$.

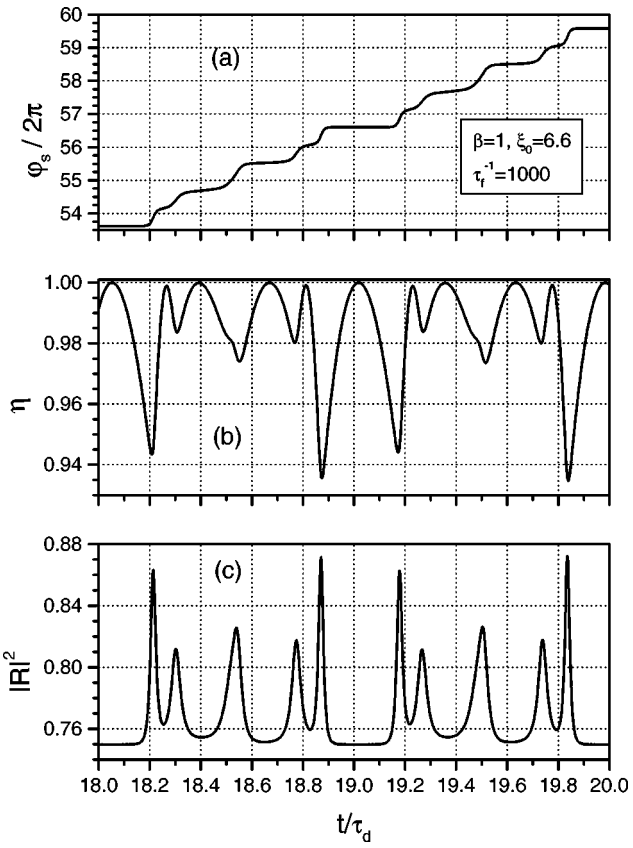

FIG. 14. Dependences $\varphi_s(\tau)$, $\eta(\tau)$, and $|R(\tau)|$ for $\xi_0=6.6$, $\beta=1$, and $18\leqslant\tau\leqslant20$.

also below. The size of the attractor is noticeably larger than earlier; this gives larger oscillations of η in the vicinity of unity. The obvious asymmetry of this attractor is due to the nonzero value of the characteristic phase θ. Since this value is very small, we should expect a strong sensitivity of the form of the attractor to various perturbations for $\beta=1$. In particular, the adiabatic decrease of τ_f changes considerably its form in contrast to the cases $\beta=4$ and 6. The large transient time, $\tau\approx30$, can also be ascribed to the high sensitivity of the system. The ''effective charge'' of this attractor $N=3$.

Figure 14 shows the dependences $\varphi_s(\tau)$, $\eta(\tau)$, and $|R(\xi_0,\tau)|^2$ within the time interval $18\leqslant\tau\leqslant20$ when the transient process is all over. Here the period $T\simeq0.97$, it is approximately three times larger than before. This complicates indeed the behavior of the above variables within a period. The average slope of $\varphi_s(\tau)$ is positive and large, $\Omega_s\simeq19.3$, the maximum distance $(1-\eta)_{max}\simeq0.07$, and the output intensity $|R(\xi_0,\tau)|^2$ shows strong eruptions above the average value $\simeq0.76$. As we have mentioned, the structure of the attractor changes noticeably during an adiabatic decrease of the feedback response time τ_f. Correspondingly, the behavior of $\varphi_s(\tau)$ looks sometimes irregular. The elements of fine structure, such as the presence of tripling and the period of oscillations, remain, however, quite robust.

The question arises about what happens if we choose other values of the beam ratio β and what kind of transitions can take place between different attractors. To give at least a partial answer to these questions, we have performed a few additional numerical experiments. First, we increased β slowly (with the rate 0.02) from 1 to 24, starting from the periodic state that corresponds to Fig. 11(c). Initially, increasing β results in a gradual convergence of the different loops of the attractor. At $\beta\simeq2$ the three-loop structure has already transformed into one loop similar to the one shown in Fig. 11(a). Correspondingly, the period tripling disappears. An apparent disappearance of the period tripling for $\varphi_s(\tau)$ and $\eta(\tau)$ occurs even earlier. The described transition is similar to the second-order phase transition or to the so-called soft excitation of oscillations [12,13]. It is not accompanied by a change of the average slope Ω_s, but the ''effective charge'' $N=3$ transforms into $N=1$.

Further increasing of β, we find gradual changes of the form of the bagel. With β approaching $\simeq6.8$ these changes accelerate and within the interval $6.8\lesssim\beta\lesssim7.3$ (which τ changing by $\Delta\tau\approx15$) the behavior of the trajectory becomes apparently irregular. Then, for $\beta\simeq7.4$, a two-loop attractor corresponding to the ''effective charge'' $N=0$ is formed, see Fig. 15. This transition has some analogy with the first-order phase transitions or with the so-called hard excitation of oscillations because it cannot be performed continuously without a sharp bend of the trajectory. It is important that the above transition is very pronounced for the time dependence $\varphi_s(\tau)$, see Fig. 16. The change of the average slope of Ω_s and of the shape (but not the period) of the oscillations is very clear despite a rather irregular behavior of the corresponding trajectories.

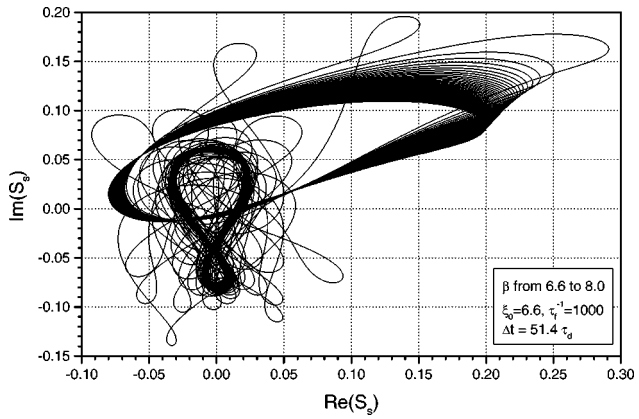

FIG. 15. Trajectory $\mathcal{S}_s(\tau)$ for $\beta(\tau)$ increasing adiabatically from 6.6 to 8. Initially, the trajectory has a bagel-like form. Then, after an apparently irregular behavior, it attains a two-loop structure.

An increase of β from $\simeq 7.5$ to $\simeq 19$ is accompanied by a gradual decrease of the size of the two-loop attractor, a reduction of its lower loop, and by a drift of its weight center to the left, see Fig. 17 and compare with Fig. 15. At $\beta \simeq 19$ the attractor crosses the zero point and acquires a one-loop shape that, however, shows a kind of spike. This transition is not accompanied by a change of the slope Ω_s. Further increasing β, the attractor becomes smoother and its size smaller. Finally, our adiabatic procedure fails because of the approach of the threshold value β^{th} and the corresponding critical slowing down [13].

With β decreasing slowly from 22 to 1 the character of the changes remains initially nearly reversed to the one described. However, the situation changes for sufficiently small values of β. The transition from the two-loop to the one-loop structure occurs only for $\beta \simeq 4.37$, i.e., some hysteresis takes place within the interval $4.37 \lesssim \beta \lesssim 6.95$. Further decrease of β does not result in a transformation of the ''bagel'' into the three-loop structure shown in Fig. 11(c). The bagel-like shape of the attractor survives up to $\beta = 1$.

Finally, we touch on the effect of the crystal thickness ξ_0 on the behavior of our nonlinear system. For $\xi_0 = 4$ we have

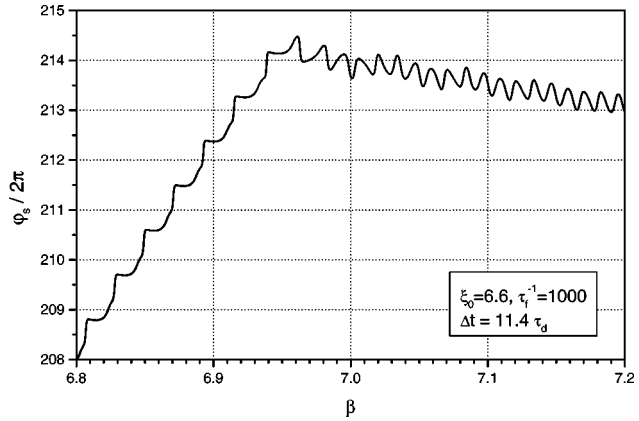

FIG. 16. Dependences $\varphi_s(\tau)$ for $\beta(\tau)$ increasing adiabatically from 6.8 to 7.2.

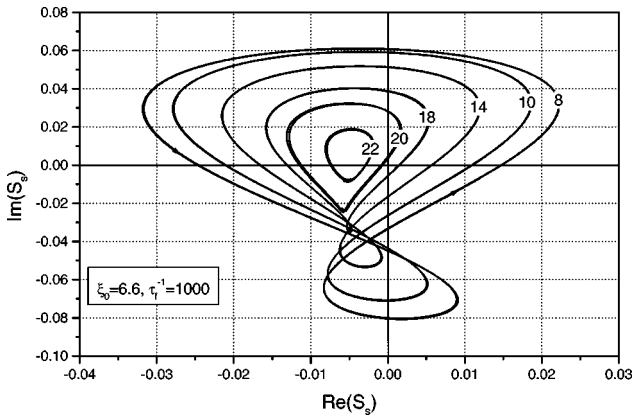

FIG. 17. Transformation of the form of the attractor for β increasing adiabatically from 7.5 to 22.

not found any bagel-like orbits. Here the attractor consists typically of two loops. For a sufficiently small beam ratio β it corresponds to period doubling and $N = 2$. For $\beta = 2$ and with ξ_0 decreasing adiabatically from 6.6 to 3.5 we have observed a pronounced one-loop→two-loop transition similar to the one shown in Fig. 15. It take place for $\xi_0 \approx 4.6$.

An adiabatic increase of ξ_0 from 6.6 to 15 has not shown any sign of an onset of chaos that could be expected from general considerations [11,12]. At $\beta = 1$, within the region $9 \lesssim \xi_0 \lesssim 9.5$, we have seen a smooth transition to a two-loop attractor with $N = 2$. Increasing ξ_0 from 9.5 to 15 has given only some gradual growth of the size of this two-loop structure and of the period of oscillation T.

VI. EXPERIMENTAL RESULTS

For sufficiently large and small beam ratios, $\beta \gtrsim 50$ and $\beta \lesssim 0.03$, we did not observe any self-oscillatory regimes with our sample at $\lambda = 532$ nm. In steady state we had here a considerable energy transfer to the weakest pump beam and the input phase φ_s linearly changing in time. The diffraction efficiency remained less than 1. These features are in good agreement with our theory if we take into account that the estimated dimensionless thickness of our sample at 532 nm is $\xi_0 \approx 8$. Some asymmetry of the above interval of the beam ratio can be referred to the influence of the diffusion charge transport.

Within the interval $0.03 < \beta < 50$ we have observed a variety of well recognizable oscillatory regimes at 532 nm with permanently working feedback and diffraction efficiency very close to 1. We believe that we have detected all the regimes described in the previous subsection.

Figure 18(a) shows a typical fragment of the feedback-controlled dependence $\varphi_s(t)$ for $\beta = 10$. A large constant average slope and quasiperiodic phase steps are clearly seen on this plot. These elements are qualitatively the same as those presented in Fig. 10(a). The time distance between subsequent steps can be estimated to be $\approx 0.2 t_d$. The dielectric relaxation time t_d is about 200 s for our experimental conditions. Next, Fig. 18(b) corresponds to $\beta = 6.6$. It shows a considerably smaller average slope and clearly pronounced quasiperiodic phase oscillations. The period of the oscilla-

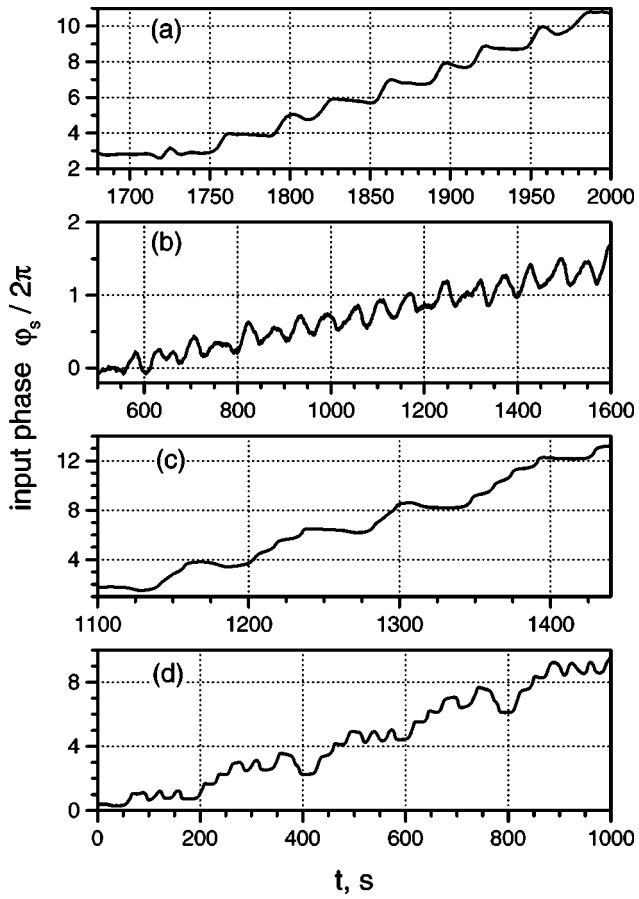

FIG. 18. Fragments of experimentally obtained feedback-controlled phase dependences $\varphi_s(t)$ at $\lambda = 532$ nm. (a) corresponds to $\beta = 10$, (b) corresponds to $\beta = 6.6$, and both (c) and (d) correspond to $\beta = 1$.

tions can be estimated as $\approx 0.3\, t_d$. These features are similar to those presented in Fig. 13(a).

Figure 18(c) shows a representative dependence $\varphi_s(t)$ for $\beta = 1$ that corresponds to period tripling, compare with Fig. 14(a). The full period, $\approx 0.82 t_d$, is approximately three times larger than it is in the previous case. Lastly, Fig. 18(d) exhibits a fragment of the time dependence that shows the intermittent behavior of the phase typical of the transient stage for $\beta = 1$. Sometimes, instead of a step up, the phase φ_s makes a step down. A similar peculiarity has been observed in our numerical simulations for $\beta \approx 1$.

At $\lambda = 633$ nm, the system also exhibits self-oscillations. However, the permissable interval of the beam ratio, $0.2 \lesssim \beta \lesssim 0.4$, is much narrower here as compared to the case $\lambda = 532$ nm. This interval corresponds to the dimensionless crystal thickness $\xi_0 \approx 4$. The main reason for this decrease is a smaller value of the photovoltaic field E_{pv} at 633 nm [10].

VII. DISCUSSION

Several particular issues of our study are worth discussion. One of our important findings is that the initially introduced ideal feedback conditions are incapable of describing the whole nonlinear evolution. We have found that taking into account the inertia of the feedback loop, characterized by a small characteristic relaxation time τ_f, is the natural way to modify the ideal conditions and to ensure a permanent operation of the system. The value of τ_f is found to be determined by the the electronic components in the feedback loop.

During the initial stage of development, when the diffraction efficiency of the spatial grating, η, is not near its ultimate value, 1 or 0, the modified (inertial) feedback equations are not much different from the ideal feedback conditions. In the developed stage, the inertia of the feedback leads to an entirely-different behavior of the governing phase Φ_s: strong anharmonic oscillations.

The inertial feedback leads to a behavior of the input phase $\varphi_s(\tau)$ that is easily recognizable in experiment, namely, to fine oscillations superimposed on an average slope. In a periodic state, the oscillation period T is found to be proportional to $\sqrt{\tau_f}$ and the average value $\langle 1 - \eta(\tau) \rangle$ to be proportional to τ_f. These results give clear predictions for experiment and rather weak restrictions on the frequency characteristics of the feedback amplifier.

An important theoretical and experimental finding is the occurrence of various periodic regimes with characteristics strongly dependent on the experimentally controlled parameters, such as input beam ratio and coupling strength. In particular, different regimes manifest themselves in different average slopes of the input phase $\varphi_s(\tau)$ and in different shapes of the oscillations.

The representation of the fundamental amplitudes by trajectories in the complex plane gives a powerful tool for the analysis of the nonlinear regimes. It allows us to classify the different attractors and to make certain judgements about transitions between them. In many respects, the correspondence between different regimes is similar to the correspondence between the high- and low-symmetry phases in the phase-transition theory.

VIII. CONCLUSIONS

Above we have given an extended introduction into the theory and experiment of a strongly nonlinear optical system, the feedback controlled photorefractive beam coupling. Being implemented experimentally several years ago, it operated till recently like a black box providing experimentators and theorists with unusual and exciting observed data. We have formulated a general theory of this nonlinear system that is free of unnecessary model assumptions but incorporates the essence of the feedback operation. For typical values of material and experimental parameters our numerical simulations have demonstrated the occurrence of a variety of qualitatively different periodic regimes (attractors) and nontrivial transitions between them. The theoretical results are in good qualitative agreement with our original experimental data for $LiNbO_3$ crystals.

[1] M. Segev *et al.*, Phys. Rev. Lett. **68**, 923 (1992); M.F. Shih, M. Segev, and G. Salamo, *ibid.* **78**, 2551 (1997); W. Krolikowski *et al.*, *ibid.* **80**, 3240 (1998).
[2] T. Honda, Opt. Lett. **18**, 598 (1993); A.V. Mamaev and M. Saffman, Phys. Rev. Lett. **80**, 3499 (1998); S.G. Odoulov *et al.*, *ibid.* **83**, 3637 (1999).
[3] B. Sturman *et al.*, J. Opt. Soc. Am. B **10**, 1919 (1993); T.E. McClelland *et al.*, Phys. Rev. Lett. **73**, 3082 (1994); H.C. Pedersen and P.M. Johansen, *ibid.* **77**, 3106 (1996).
[4] A. Freschi and J. Frejlich, J. Opt. Soc. Am. B **11**, 1837 (1994).
[5] P.M. Garcia, K. Buse, D. Kip, and J. Frejlich, Opt. Commun. **117**, 35 (1995).
[6] P.M. Garcia, A.A. Freschi, J. Frejlich, and E. Krätzig, Appl. Phys. B: Lasers Opt. **63**, 207 (1996).
[7] V.P. Kamenov, K.H. Ringhofer, B.I. Sturman, and J. Frejlich, Phys. Rev. A **56**, R2541 (1997).
[8] K.H. Ringhofer, V.P. Kamenov, B.I. Sturman, and A.I. Chernykh, Phys. Rev. E **61**, 2029 (2000).
[9] L. Solymar, D.J. Webb, and A. Grunnet-Jepsen, *The Physics and Applications of Photorefractive Materials* (Clarendon Press, Oxford, 1996).
[10] B.I. Sturman and V.M. Fridkin, *The Photovoltaic and Photorefractive Effects in Noncentrosymmetric Materials* (Gordon and Breach Publishers, Philadelphia, 1992).
[11] E. Ott, *Chaos in Dynamical Systems* (Cambridge University Press, Cambridge, 1997).
[12] H. Haken, *Advanced Synergetics* (Springer-Verlag, Berlin, 1983).
[13] L.D. Landau and E.M. Lifshitz, *Statistical Physics* (Pergamon Press, Oxford, 1980).